Supplementary Information
for
Two Highly Stable Isoreticular M_8-pyrazolate (M = Co, Ni) Metal-Organic Frameworks for CO_2 Conversion

Fa-Xue Ma,[a,b] Lei-Yan Lyu,[a,c,d] Jiawei Chen,[b] Tao Huang,[a] Teng Zhang*[a,d,e] and Rong Cao*[a,b,d,e]

[a] State Key Laboratory of Structural Chemistry, Fujian Institute of Research on the Structure of Matter, Chinese Academy of Sciences, Fuzhou 350002, China.

[b] College of Chemistry and Chemical Engineering, Xiamen University, Xiamen 361005, China.

[c] College of Chemistry and Materials Science, Fujian Normal University, Fuzhou 350007, China

[d] Fujian College, University of the Chinese Academy of Sciences, Fuzhou 350002, China

[e] University of the Chinese Academy of Sciences, Beijing 100049, China.

* Email: zhangteng@fjirsm.ac.cn (T.Z.); rcao@fjirsm.ac.cn (R.C.)

1. Reagents and apparatus.

All chemicals and reagents were used as received from commercial sources without further purification. Powder X-ray diffraction (PXRD) patterns were recorded on a Miniflex 600 diffractometer using Cu Kα radiation (λ = 0.154 nm). SEM images were taken with an SU-8010 field emission scanning electron microscope with the secondary electron imaging resolution ≤ 1 nm (15 kV, XWD ≥ 4 mm) or ≤ 1.3 nm (1 kV). N_2 sorption isotherms were measured by a Micromeritics ASAP 2460 instrument. CO_2 sorption isotherms were measured by a Micrometrics ASAP 2020 instrument. X-ray photoelectron spectroscopy (XPS) measurements were performed on an ESCALAB 250Xi X-ray photoelectron spectrometer (Thermo Fisher) using an Al K*α* source (15 kV, 10 mA). Thermogravimetric analyses (TG) was conducted with a Netzsch STA449F3 instrument with an Al_2O_3 crucible at a heating rate of 10 °C/min under nitrogen atmosphere. ^{1}H NMR (400 MHz) spectra were recorded on a Bruker AVANCE III HD 400 spectrometer and referenced to the proton resonance from incomplete deuteration of the deuterated chloroform (δ 7.26) or deuterated DMSO (δ 2.50). The molecular weight and molecular weight distribution of the polymer products were determined by gel permeation chromatography (GPC) at 35 °C in polystyrene standard on a Waters 410 GPC instrument with THF as the eluent, where the flow rate was set at 1.0 mL min^{-1}.

2. Synthesis of the ligand and MOFs.

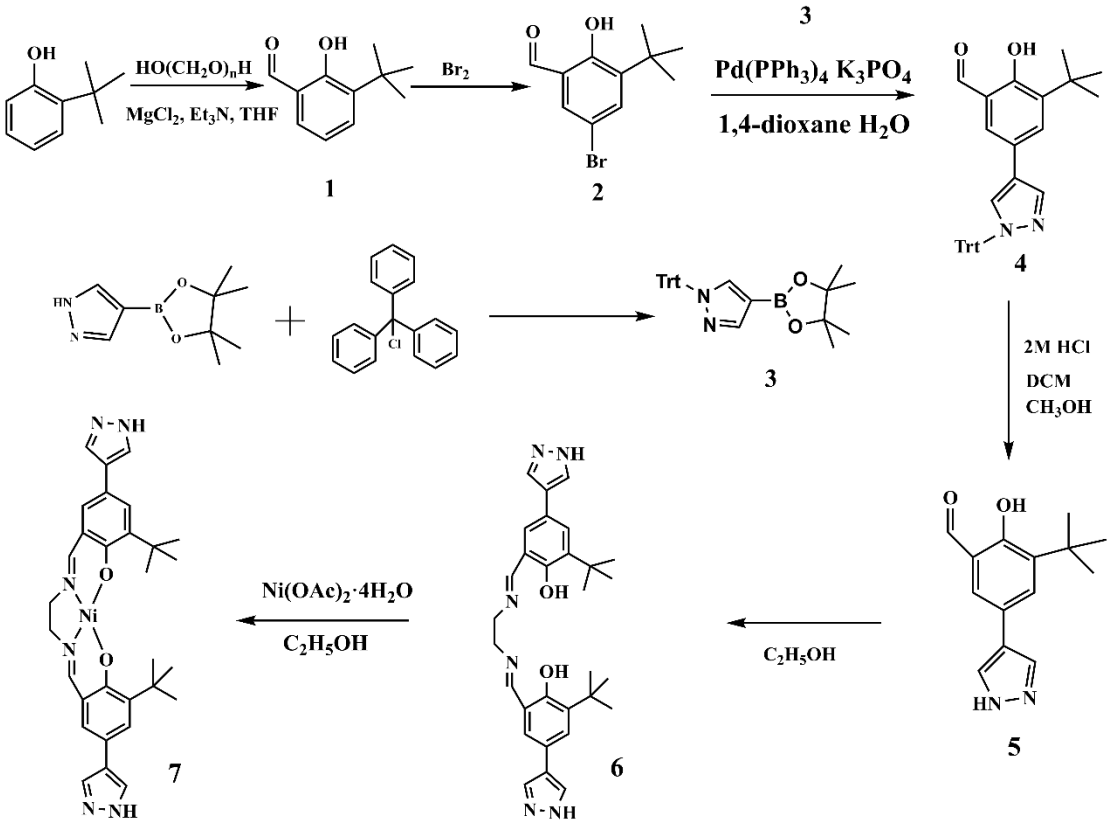

Scheme S1. Synthesis of H_2L^{Ni} Ligand.

The H_2L^{Ni} ligand was synthesized following a previous literature procedure[1]. ^{1}H NMR (400 MHz, DMSO-d_6) δ 12.77 (s, 1H), 7.88 (s, 2H), 7.75 (br s, 1H), 7.32 (d, J = 4.0 Hz, 2H), 3.42 (s, 2H), 1.36 (s, 9H).

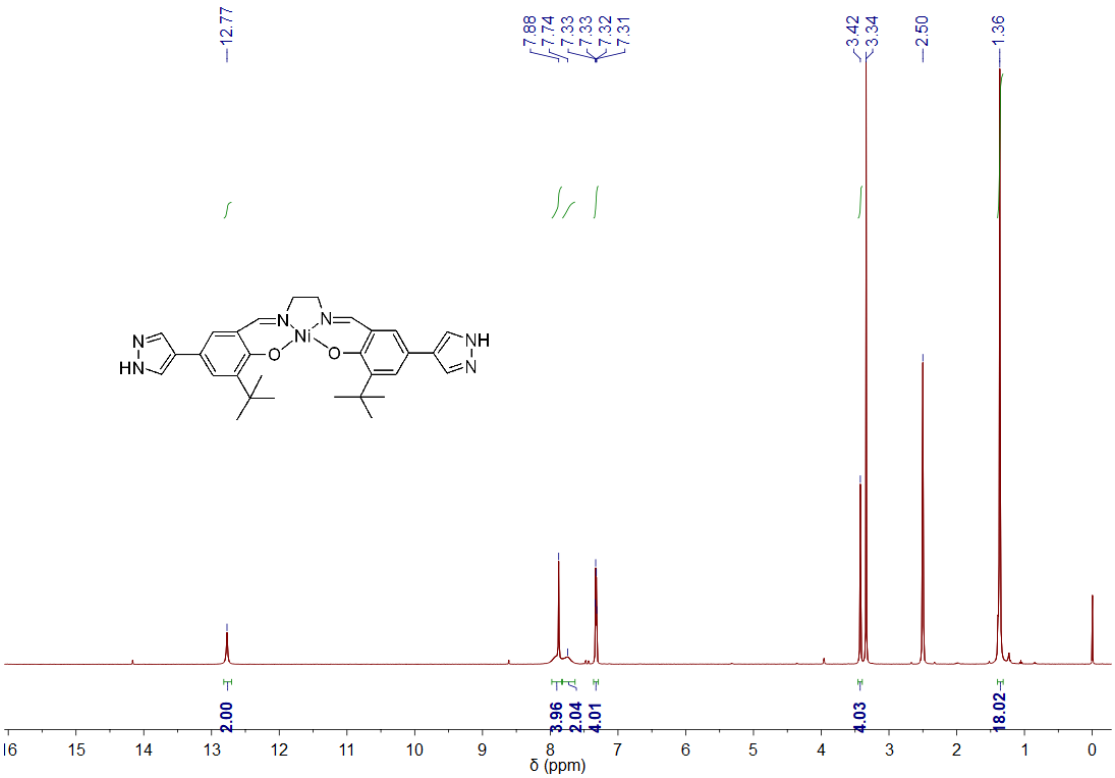

Figure S1. ^{1}H NMR spectrum (400 MHz, DMSO-d_6) of $H_2\mathbf{L}^{\mathbf{Ni}}$.

FICN-18. $H_2\mathbf{L}^{\mathbf{Ni}}$ (5 mg) and $Ni(OAc)_2{\cdot}4H_2O$ (10 mg) were dissolved in 4 mL DMF/H_2O (v:v = 1:1) mix solvent, sealed in a 10 mL glass bottle and then heated at 110°C for 72 h in an oven. The dark red octahedral crystals of **FICN-18** were collected by filtration after cooling down, washed with DMF, CH_3OH and acetone, subsequently, and dried at 70°C for 10 h (yield: 80% based on $H_2\mathbf{L}^{\mathbf{Ni}}$).

FICN-19. $H_2\mathbf{L}^{\mathbf{Ni}}$ (5 mg) and $Co(OAc)_2{\cdot}4H_2O$ (30 mg) were dissolved in 5 mL DMF/H_2O (v:v = 3:2) mix solvent, sealed in a 10 mL glass bottle and then heated at 110°C for 72 h in an oven. The dark red octahedral crystals of **FICN-19** were collected by filtration after cooling down, washed with DMF, CH_3OH and acetone, subsequently, and dried at 70°C for 10 h (yield: 37% based on $H_2\mathbf{L}^{\mathbf{Ni}}$).

3. Single crystal X-ray crystallography.

Single crystal X-ray diffraction (SCXRD) of compound FICN-18 was performed with a BRUKER D8 VENTURE equipped with Cu-Kα and Mo-Kα radiation at 150 K. Mo Kα radiation was used. SCXRD of FICN-19 was performed with a BRUKER D8 VENTURE equipped with Cu-Kα radiation (λ = 0.154 nm). The frames were integrated with the Bruker SAINT© build in APEX III software package using a narrow-frame integration algorithm, which also corrects for the Lorentz and polarization effects. Absorption corrections were applied using SADABS. Structures were solved by intrinsic phasing and refined to convergence by least squares method on F^2 using the SHELX-2019 software suite. Scattering from the highly disorder guest molecules was modelled by the SQUEEZE program in PLATON software suite. All non-hydrogen atoms are refined anisotropically.

Table S1. Crystallographic data of FICN-18 and FICN-19

Name	FICN-18	FICN-19
Empirical formula	$C_{90}H_{96}N_{18}Ni_7O_9$	$C_{90}H_{96}Co_4N_{18}Ni_3O_9$
Formula weight	1984.69	1985.77

Temperature/K	149.95	150
Crystal system	cubic	cubic
Space group	Fd-3m	Fd-3m
a/Å	36.791(3)	36.8381(3)
b/Å	36.791(3)	36.8381(3)
c/Å	36.791(3)	36.8381(3)
α/°	90	90
β/°	90	90
γ/°	90	90
Volume/Å^3	49801(13)	49991.0(12)
Z	16	16
ρ_{calc}(g/cm^3)	1.062	1.055
μ/mm^{-1}	1.084	4.925
F(000)	16576	16416
Radiation	Mo Kα (λ = 0.71073 Å)	Cu Kα (λ = 1.54178 Å)
2θ range for data collection/°	4.428 to 54.97	7.96 to 144.82
Index ranges	$-47 \le h \le 33$, $-44 \le k \le 45$, $-47 \le l \le 46$	$-30 \le h \le 41$, $-18 \le k \le 44$, $-29 \le l \le 30$
Reflections collected	62713	10536
Independent reflections	2700 [R_{int} = 0.0795, R_{sigma} = 0.0246]	2335 [R_{int} = 0.1075, R_{sigma} = 0.0549]
Data/restraints/parameters	2700/126/168	2335/66/144
Goodness-of-fit on F^2	1.066	1.041
Final R indexes [I>=2σ (I)]	R_1 = 0.0489, wR_2 = 0.1285	R_1 = 0.0977, wR_2 = 0.2555
Final R indexes [all data]	R_1 = 0.0618, wR_2 = 0.1396	R_1 = 0.1335, wR_2 = 0.2852
Largest diff. peak/hole / e Å^{-3}	0.69/-1.02	1.80/-0.92

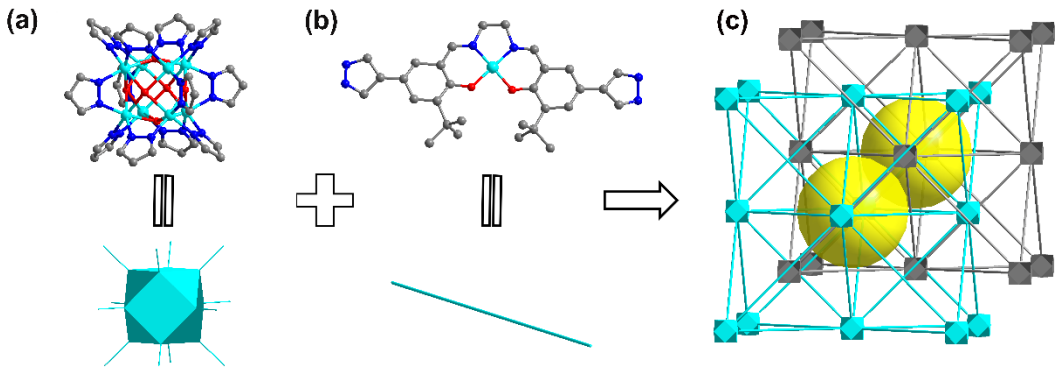

Figure S2. Construction of the FICN-18 and FICN-19: (a) the $M_8(OH)_4(H_2O)_2(pyz)_{12}$ node (Ni or Co: turquoise; N: blue; O: red); (b) the Ni(salen)derived bis(pyrazolate) ligand (Ni: turquoise); (c) two-fold interpenetration structure of FICN-18 and FICN-19.

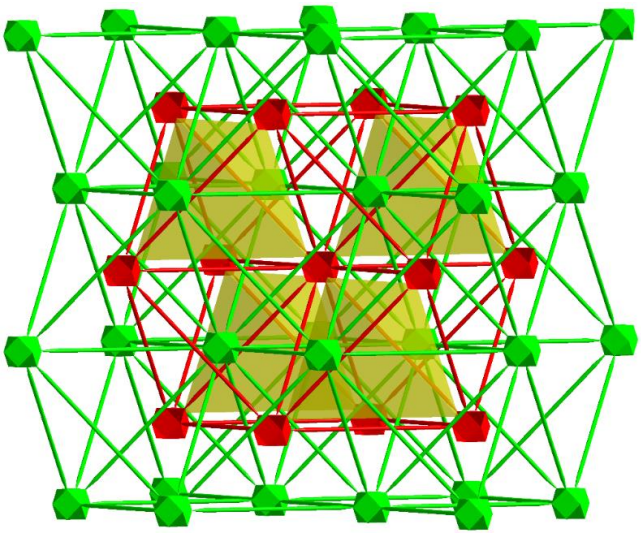

Figure S3. The $M_8(OH)_4(H_2O)_2$ (M = Ni, Co) cluster of one network locates in the tetrahedral cavity formed by the other network with 50% occupancy.

4. Additional characterizations of pristine FICN-18 and FICN-19.

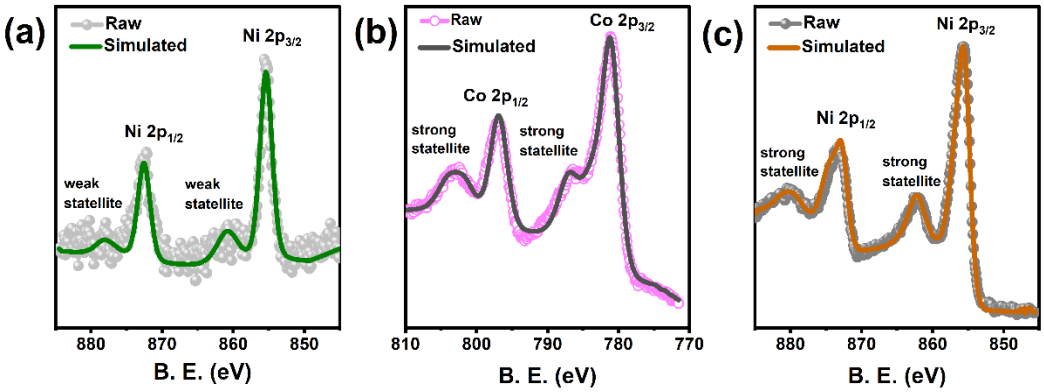

Figure S4. (a) Co and (b) Ni 2p XPS spectra of FICN-19; (c) Ni 2p XPS spectra of FICN-18.

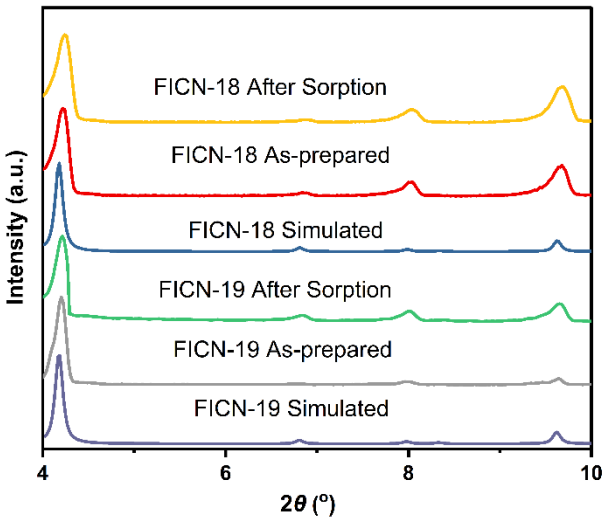

Figure S5. PXRD patterns of as-prepared and after N_2 sorption MOFs FICN-18 and FICN-19 (magnified for 2θ = 4-10°).

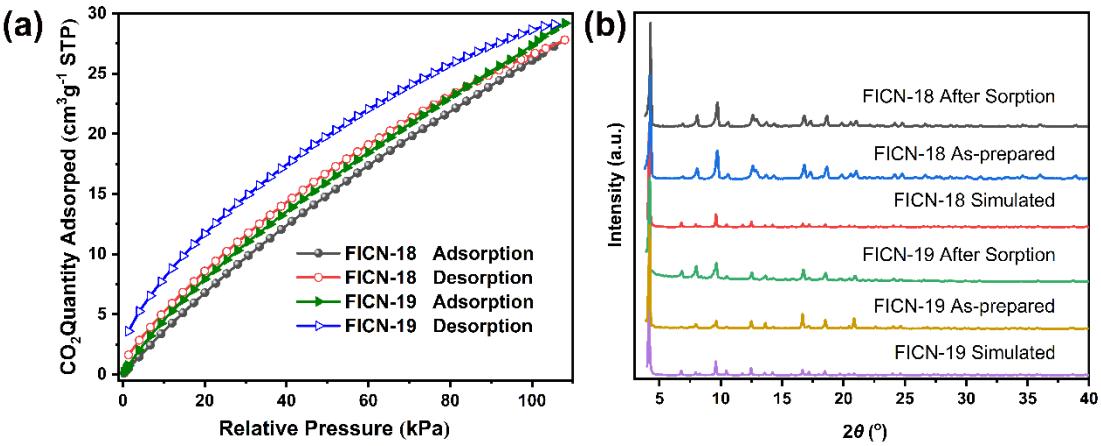

Figure S6. (a) CO_2 sorption isotherms of two MOFs at 298 K; (b) PXRD patterns before and after CO_2 adsorption/desorption test of two MOFs.

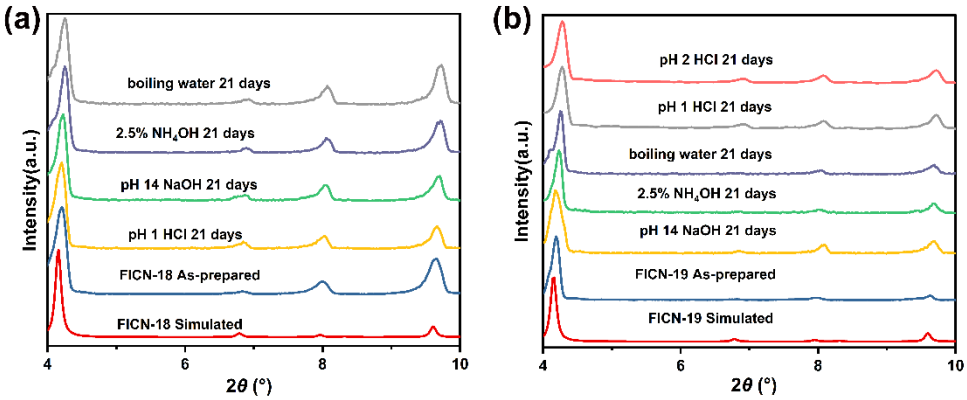

Figure S7. PXRD patterns of the as-prepared and after-treatment FICN-18 and FICN-19 MOFs (magnified for 2θ = 4-10°).

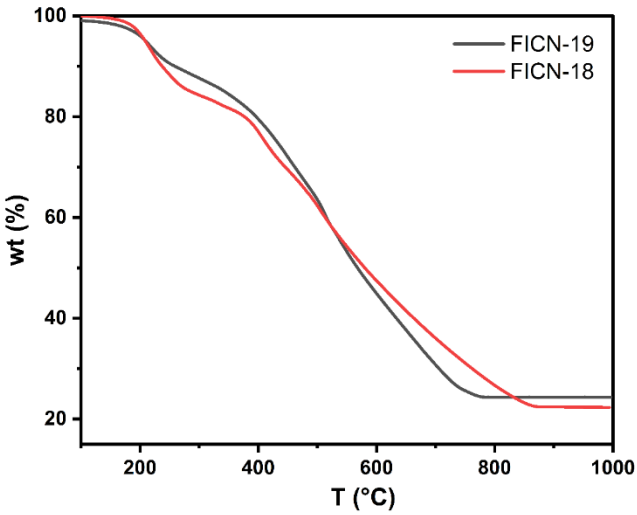

Figure S8. Thermogravimetric curves of two MOFs.

5. Comparison of FICN-18/FICN-19 with chemical stable MOFs in literature.

Table S2. Chemical stability of selected MOFs in literature reports.

MOF	Linker	Crystallinity	Assessment condition	Ref.
PCN-202(Ni)-Hf(Zr,Ni,Hf)	multi-component	Well-retained	pH = 12, 1 day	2
PCN-224(Ni)	carboxylate	Well-retained	pH = 11 (NaOH), 1 day	3
PCN-602(Ni)	pyrazolate	Well-retained	pH = 4 HCl, 1 M NaOH, RT, 1 day	4
PCN-601(Ni)	pyrazolate	Well-retained	saturated NaOH, 100 °C, 1 day	5
BUT-32(Ni) BUT-33(Ni)	pyrazolate	Well-retained	4 M KOH, RT, 1 day	6
BUT-123(Ni)	pyrazolate	Well-retained	1 M NaOH, RT, 1 day	7
$Ni_3(BTP)_2$	pyrazolate	Well-retained	pH = 14 (NaOH), 100 °C, 14 days	8
MOF-74(Ni)	2,5-dihydroxyterephthalicacid	7% FWHM decrease	pH= 13 (NaOH), RT, 1 day	9
$Ni_2Cl_2(BTDD)$	azolate	11% FWHM increase	pH= 10 (NaOH), RT, 1 day	
Ni(BDP)	azolate	18% FWHM decrease	pH= 13 (NaOH), RT, 1 day	9
Ni-HAB	hexaaminobenzene	Well-retained	Saturated NH_4OH/KOH, 100 °C, 1 day	10
NiL1	pyrazolate	Well-retained	10 M NaOH, 1 day	11
NiL1-300		Well-retained	15 M NaOH, 1 day	
[Ni(BPEB)]	pyrazolate	Well-retained	pH = 9, RT, 8 hours	12
BUT-75	multi-component	Well-retained	pH = 3 - 12, boiling water, 1 day	13
BUT-85	multi-component	Well-retained	pH = 3 - 13, 1 day	14
FICN-18/19	pyrazolate	Well-retained	pH =1-14 RT, boiling water, 21 days	**This work**

6. Additional details and data for catalytic tests.

Representative procedure for catalysis. MOF catalyst (0.04 g, 0.01 mmol; 0.06 mmol w.r.t. Ni(salen) centre), TBAB co-catalyst (0.019 g, 0.06 mmol) and epoxide substrate (6 mmol) were loaded to a 10 mL liner and placed in a high-pressure reactor and charged with CO_2 (10 atm). The reactor was then heated to 100 °C for 9 hours. After reaction, the CO_2 gas was released and the reaction mixture was filtered and washed with CH_2Cl_2 to recover MOF catalyst. The filtrate was then passed through a short column and concentrated to give the crude product. Yields of desired carbonate products were determined by adding mesitylene internal standard (278 μL, 2 mmol) to the crude products and recording the ^{1}H NMR spectra.

Recycle experiments. MOF catalysts recovered from catalysis were washed with CH_2Cl_2 for three times and dried in a vacuum oven at 50 °C for 1 h, then directly used in next catalytic cycle.

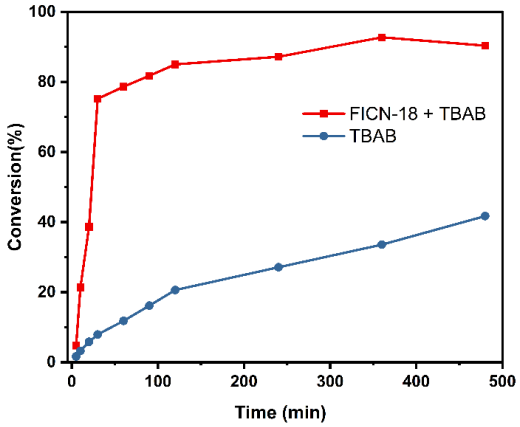

Figure S9. Time-conversion curves of styrene oxide with FICN-18/TBAB and TBAB-only catalysts.

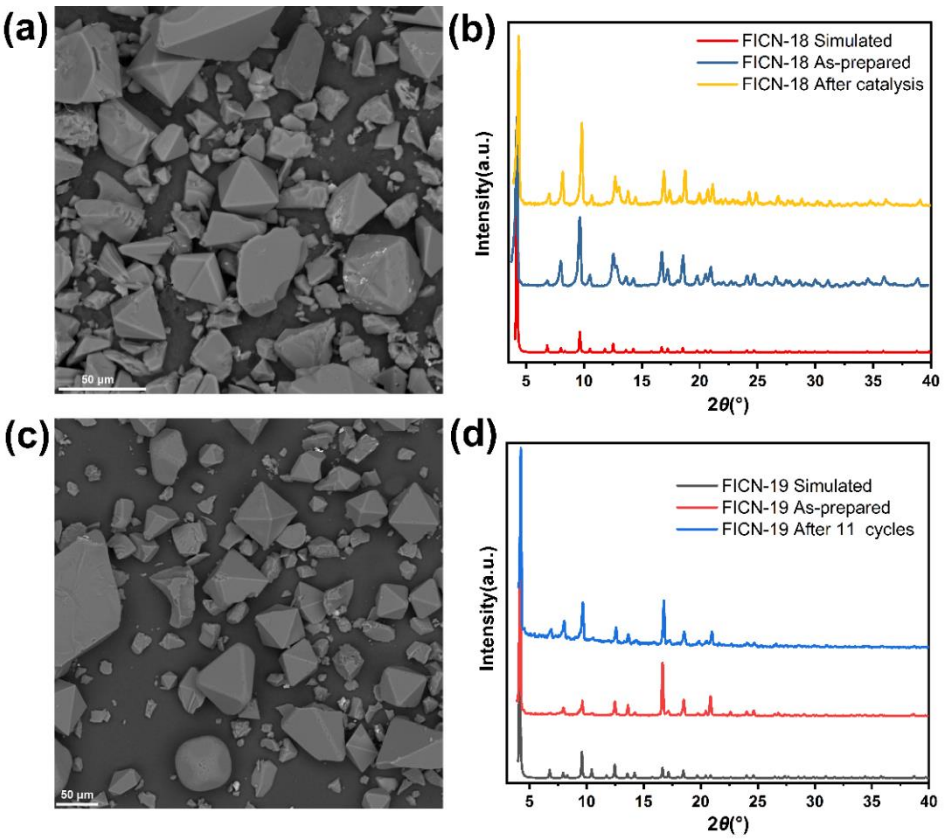

Figure S10. SEM and of PXRD patterns of FICN-18 (a, b) and FICN-19 (c, d) after catalysis.

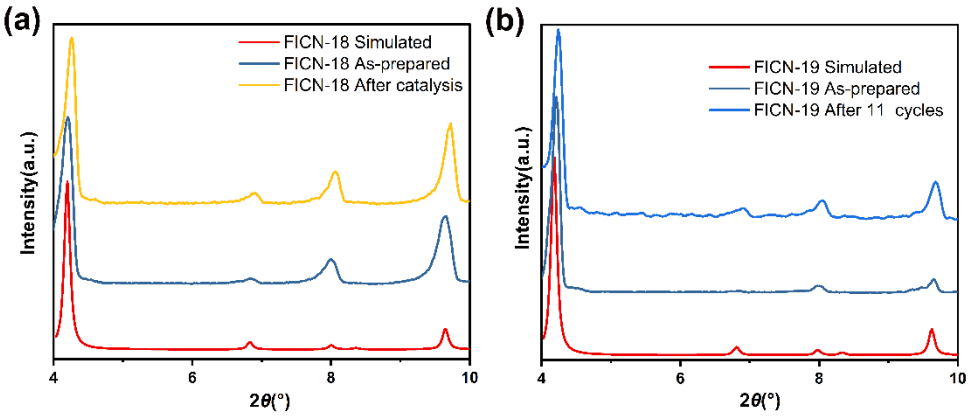

Figure S11. PXRD patterns of FICN-18 (a) and FICN-19 (b) after catalysis (magnified for 2θ = 4-10°).

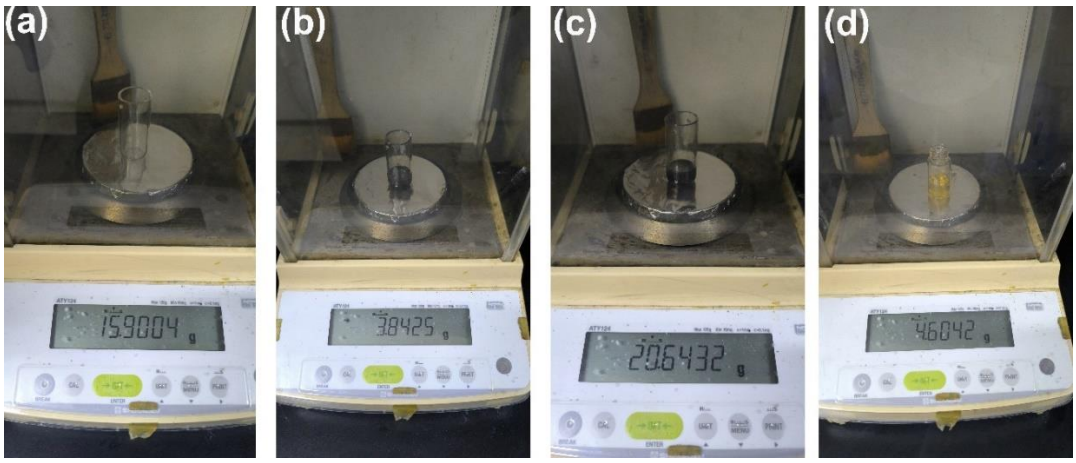

Figure S12. Photographs for gram-scale catalytic cycloaddition of styrene oxide and CO_2: (a) mass of the liner; (b) mass of styrene oxide (30 mmol, 3.6 g), TBAB (0.3 mmol, 0.08 g) and FICN-18 (0.05 mmol, 0.17 g; 0.3 mmol w.r.t. Ni(salen) centre); (c) mass of reaction mixture and liner after reaction; (d) the mass of isolated styrene carbonate product (4.6 g, 28.0 mmol, 93%).

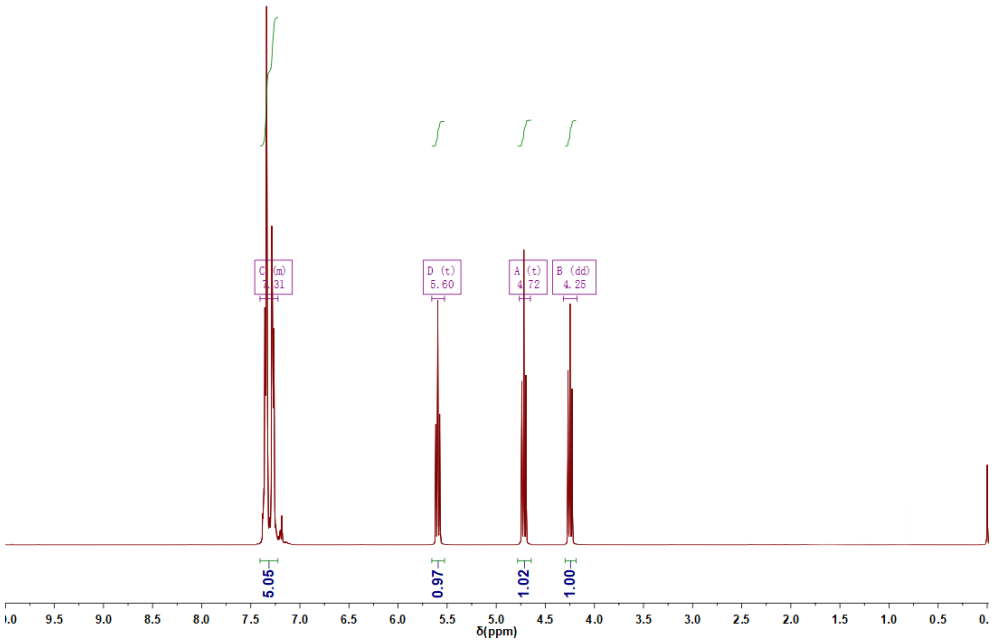

Figure S13. ^{1}H NMR ($CDCl_3$) spectrum of styrene carbonate from gram-scale synthesis.

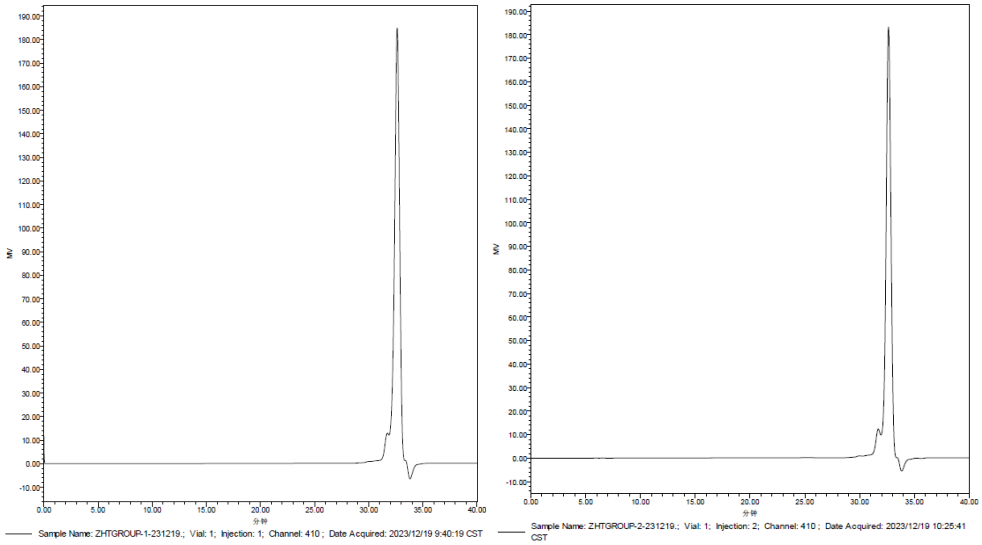

Figure S14. GPC traces of crude styrene carbonate (left) and crude cyclohexene carbonate (right) produced with FICN-18 and TBAB co-catalyst (Entry 3 and 7, Table 2). The results showed that no polymer was detected.

Table S3. CO_2/styrene oxide cycloaddition catalyzed by FICN-18 with different pressure**.**

Entry	Catalyst: co-catalyst: styrene oxide	Catalyst	P (atm)	T (°C)	Yields (%)
1	1:1:100	FICN-18	10	100	93
2	1:1:100	FICN-18	7	100	82
3	1:1:100	FICN-18	4	100	56
4	1:1:100	FICN-18	1	100	12

Table S4. CO_2 cycloaddition reactions with epoxide substrates of different sizes.

Entry	Substrate	Yields with FICN-18 (%)	Yields with FICN-19 (%)
1		99	99
2		55	26
3	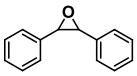	12	7

Reaction conditions: MOF catalyst (1 mol % metallosalen sites), TBAB co-catalyst (1 mol %), 10 atm CO_2, 80 °C, THF. Yields determined by ^{1}H NMR with mesitylene internal standard.

7. Comparison of FICN-18/FICN-19 with other MOF catalysts for the cycloaddition reaction of CO_2 with Styrene oxide in literature.

Table S5. Catalytic performances of **FICN-18/FICN-19** and other catalysts for the cycloaddition reaction of CO_2 with styrene oxide

Catalysts	co-catalysts	Time (h)	T (°C)	P (atm)	Yield (%)	References
MMPF-9 1.25%	TBAB 22%	48	25	1	80.3	15
$\{[Ba_3L_2(NMP)_2(H_2O)_2]\cdot 2NMP\cdot H_2O\}_n$ 1%	TBAB 10%	4	80	1	87.8	16
$[(CH_3)_2NH_2][Zn_{1.5}(\mu_3\text{-}O)_{0.5}(F\text{-}tzba)_{1.25}(bpy)_{0.25}(\mu_2\text{-}F)_{0.5}]\cdot 2DMF\cdot 2H_2O$ 1%	TBAB 10%	4	80	20	87	17
JLU-MOF58 0.1%	TBAB 5%	24	80	1	95	18
$[Dy_2Zn_2L_4(OAc)_2(MeOH)_5(H_2O)]\cdot(solvent)_n$ 0.01%	TBAB 0.75%	1	120	10	95	19
$\{[Eu(BTB)(phen)]\cdot 4.5DMF\cdot 2H_2O\}_n$ 3.5%	TBAB 5%	12	70	1	99	20
Nu-1000 4%	TBAB 10%	56	25	1	46	21
BSPOPs-Co 0.2%	TBAB 4%	18	25	1	13	22
$Zn_4Tb_3L_4$ 1.25%	TBAB 3.6%	48	25	1	76	23
SH4-Al(Cl) 0.25%	$[ClC_6Im][HCO_3]$ 0.25%	24	25	10	88	24
MOF-892/MOF-893/MOF-894 0.32%	TBAB 1%	16	80	1	82/63/66	25
$[Co_2L_{0.5}V_4O_{12}]\cdot 3DMF\cdot 5H_2O$ 1%	TBAB 0.25%	12	80	1	87	26
FICN-18 1%	TBAB 1%	9	100	9	93	**This Work**
FICN-19 1%					96	

8. ^{1}H NMR spectra of cycloaddition products.

Peak assignments of ^{1}H NMR spectra ($CDCl_3$) of cycloaddition products were compared with literature results.[19, 23, 27, 28]

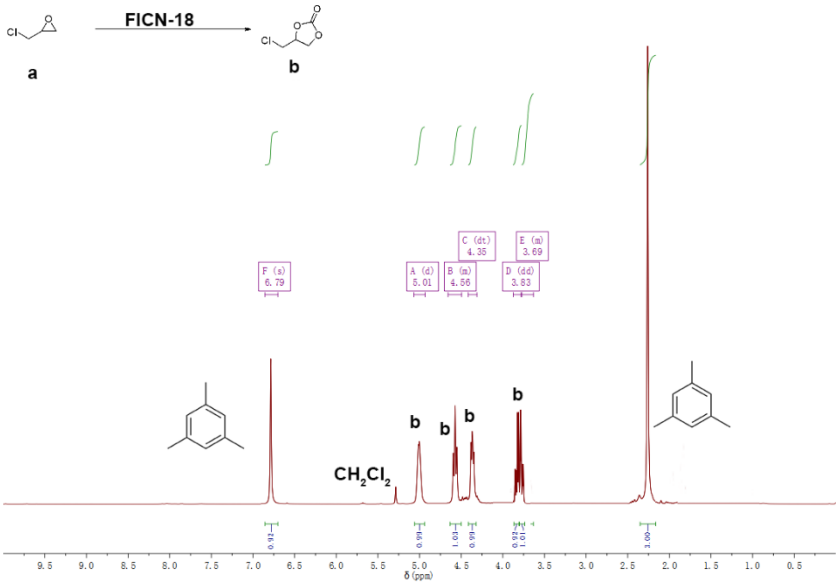

Figure S15. ^{1}H-NMR ($CDCl_3$) spectrum for crude reaction mixture of CO_2/epichlorohydrin cycloaddition catalyzed by FICN-18.

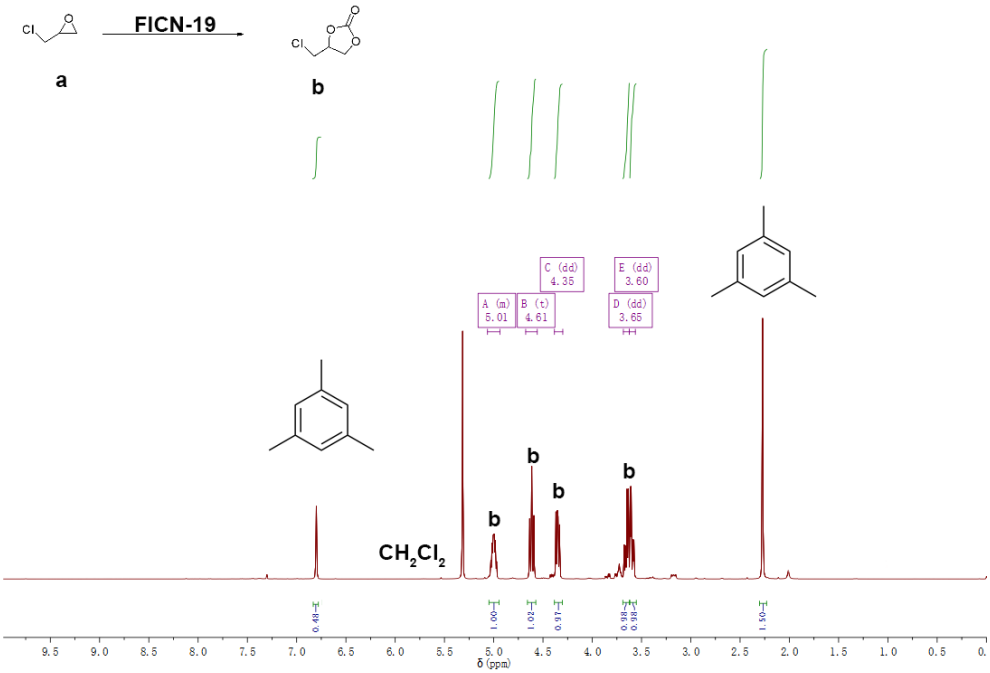

Figure S16. ^{1}H-NMR ($CDCl_3$) spectrum for crude reaction mixture of CO_2/epichlorohydrin cycloaddition catalyzed by FICN-19.

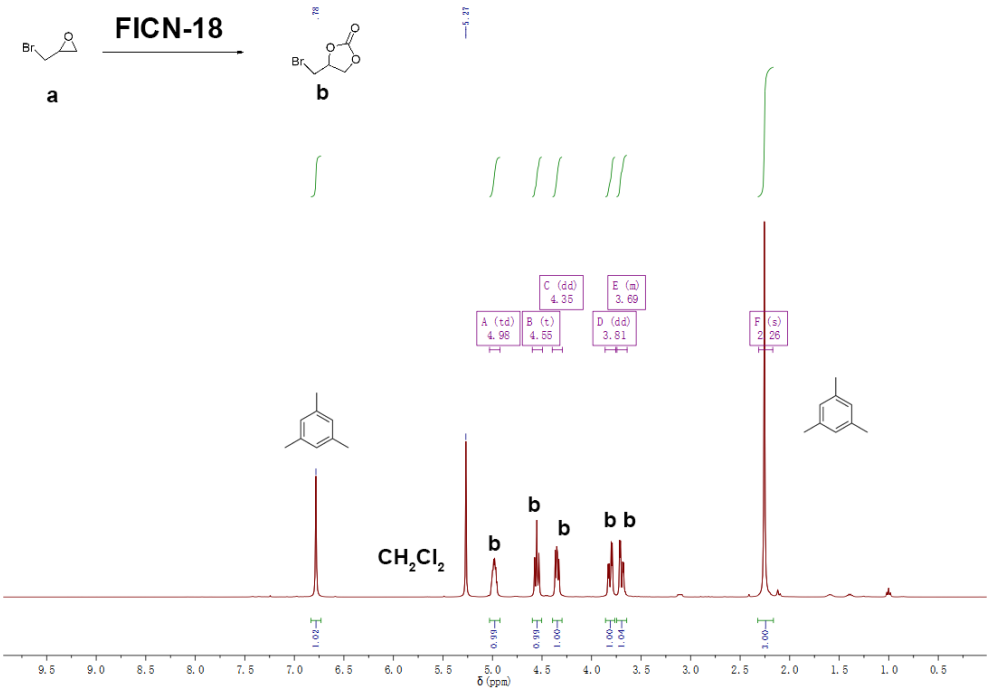

Figure S17. ^{1}H-NMR ($CDCl_3$) spectrum for crude reaction mixture of CO_2/1-bromo-2,3-epoxypropane cycloaddition catalyzed by FICN-18.

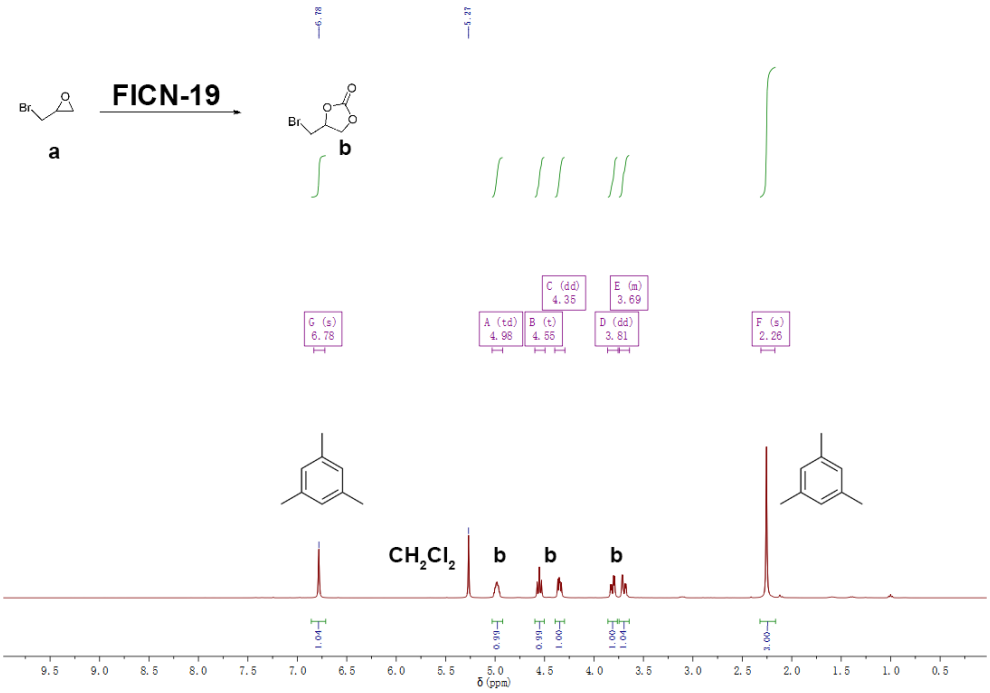

Figure S18. ^{1}H-NMR ($CDCl_3$) spectrum for crude reaction mixture of CO_2/1-bromo-2,3-epoxypropane cycloaddition catalyzed by FICN-19.

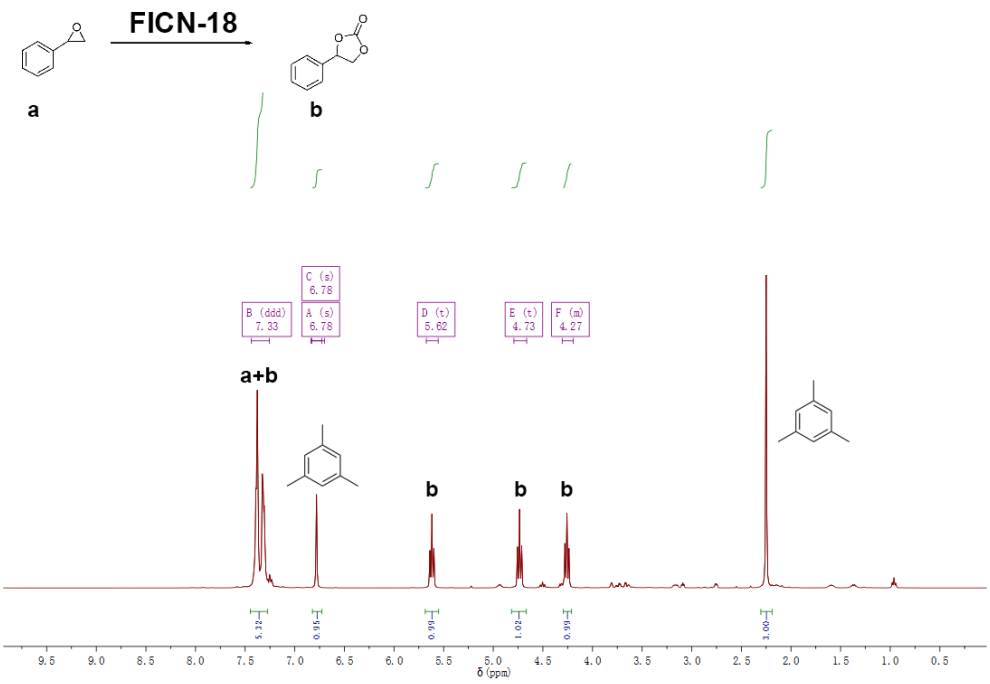

Figure S19. ^{1}H-NMR ($CDCl_3$) spectrum for crude reaction mixture of CO_2/styrene oxide cycloaddition catalyzed by FICN-18.

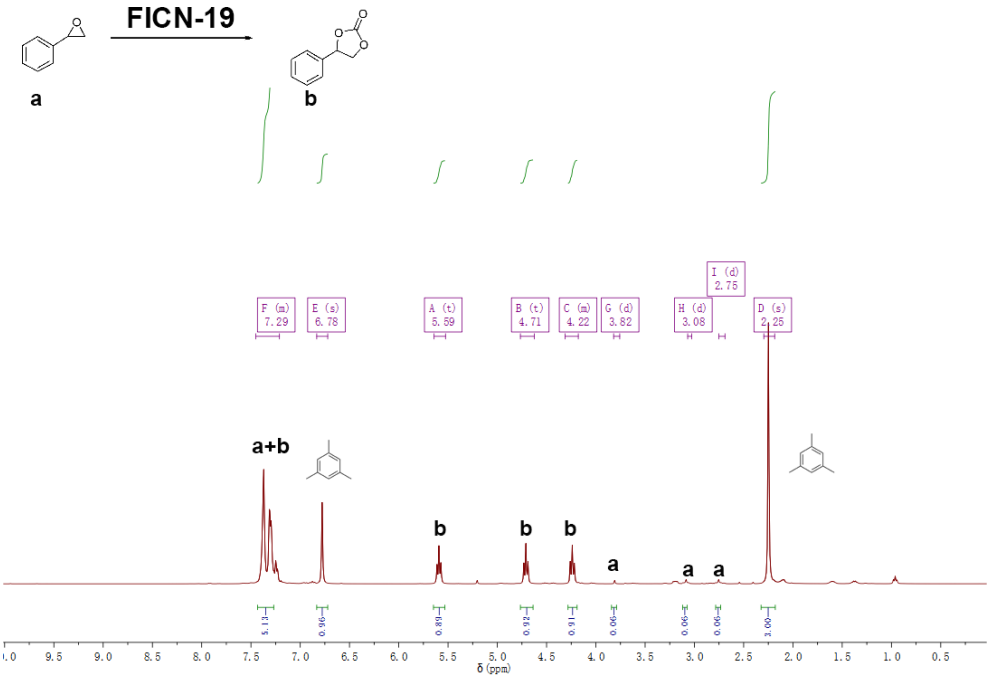

Figure S20. ^{1}H-NMR ($CDCl_3$) spectrum for crude reaction mixture of CO_2/styrene oxide cycloaddition catalyzed by FICN-19.

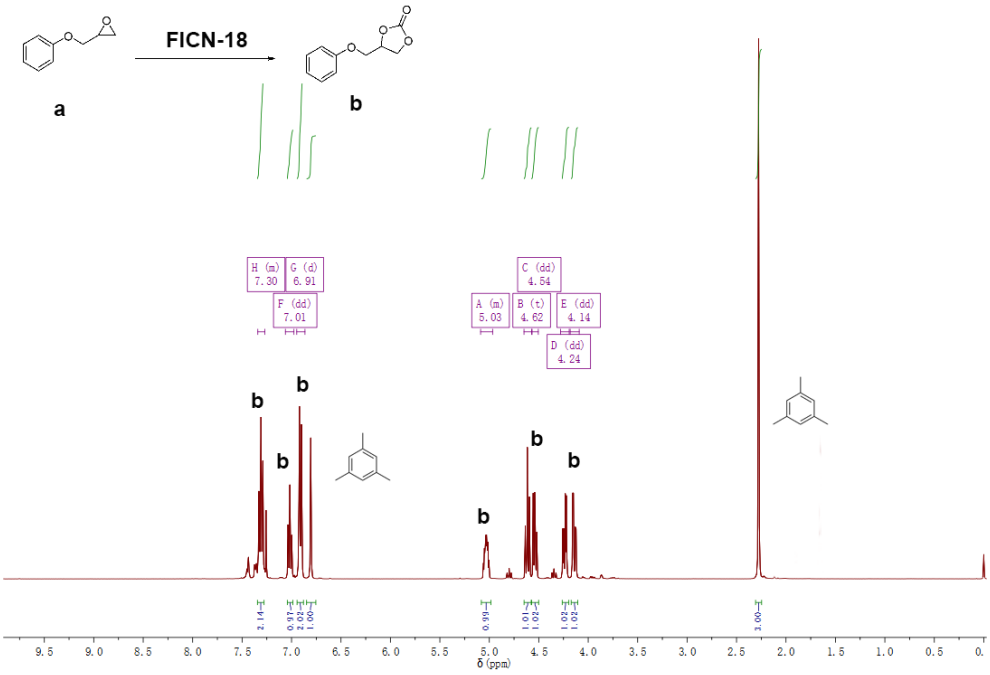

Figure S21. ^{1}H-NMR ($CDCl_3$) spectrum for crude reaction mixture of CO_2/glycidyl phenyl ether cycloaddition catalyzed by FICN-18.

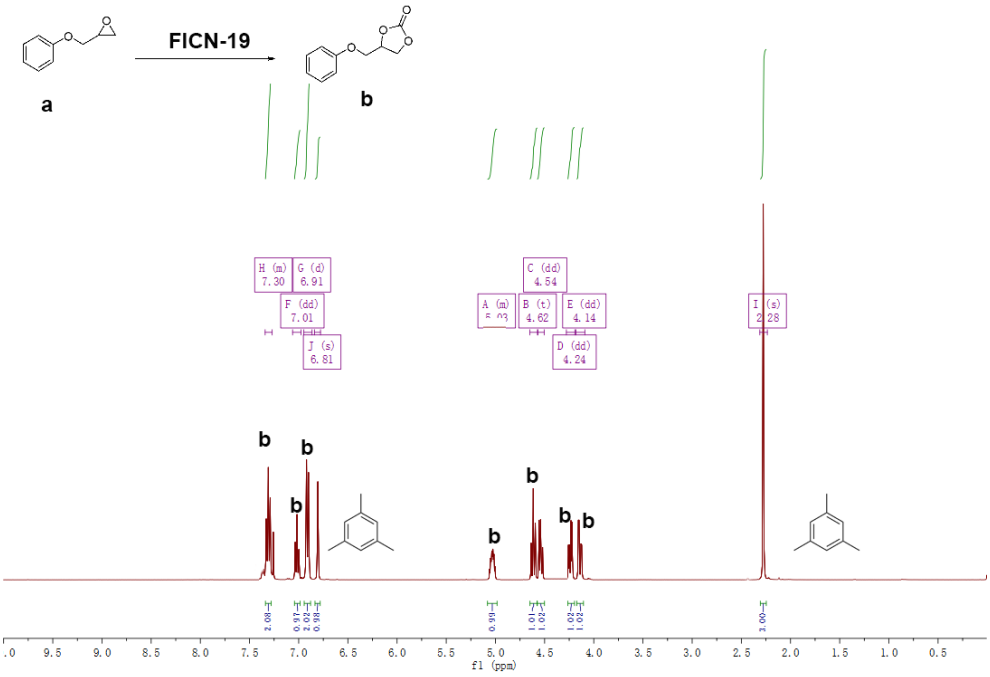

Figure S22. ^{1}H-NMR ($CDCl_3$) spectrum for crude reaction mixture of CO_2/glycidyl phenyl ether cycloaddition catalyzed by FICN-19.

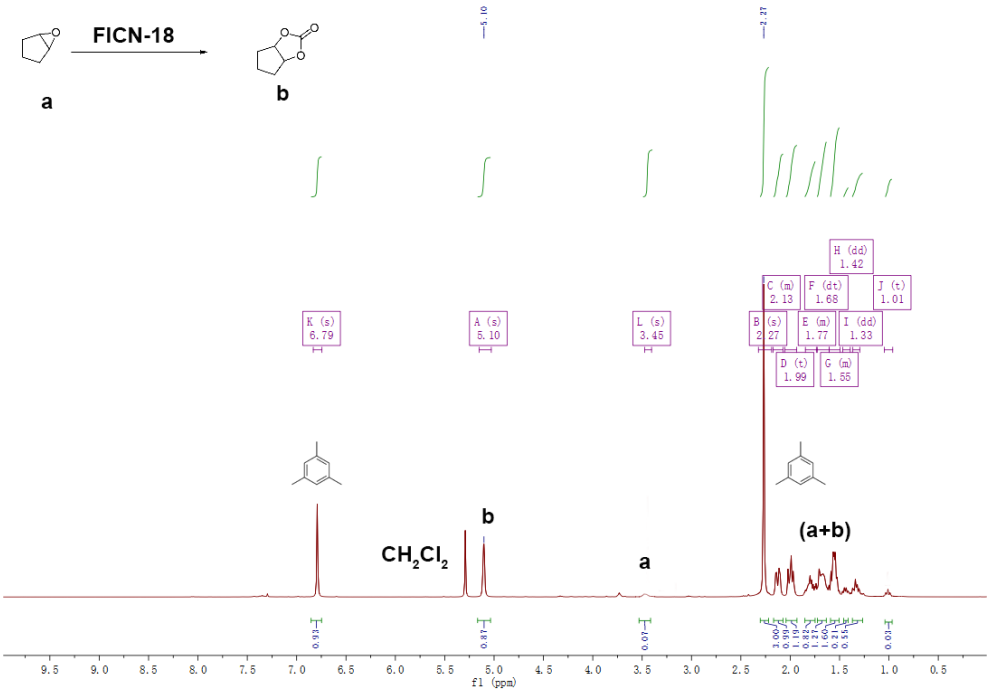

Figure S23. ^{1}H-NMR ($CDCl_3$) spectrum for crude reaction mixture of CO_2/cyclopentene oxide cycloaddition catalyzed by FICN-18.

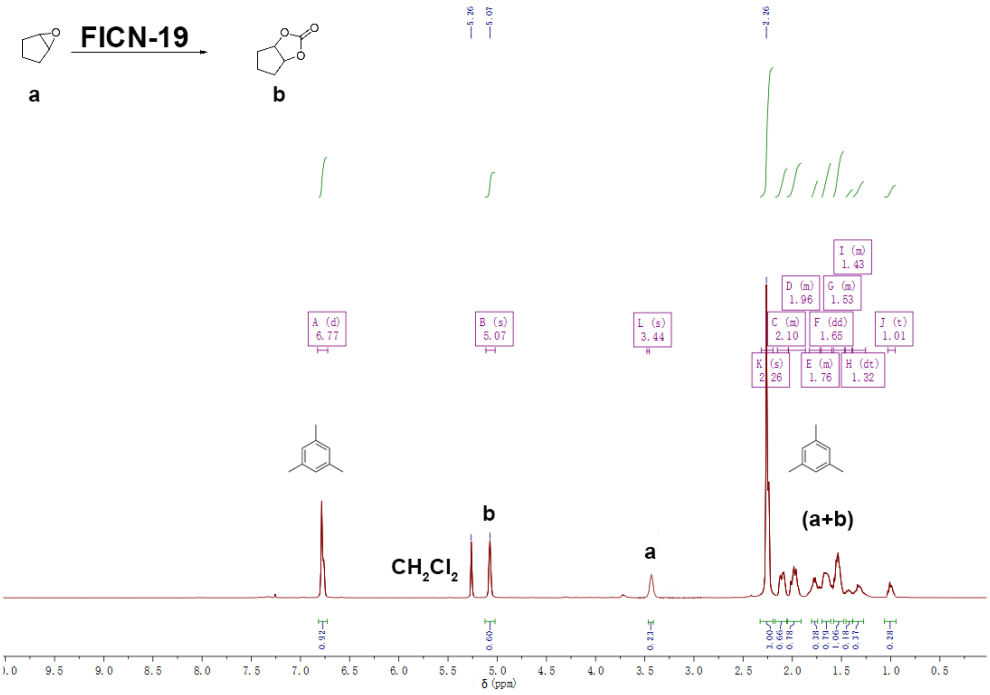

Figure S24. ^{1}H-NMR ($CDCl_3$) spectrum for crude reaction mixture of CO_2/cyclopentene oxide cycloaddition catalyzed by FICN-19.

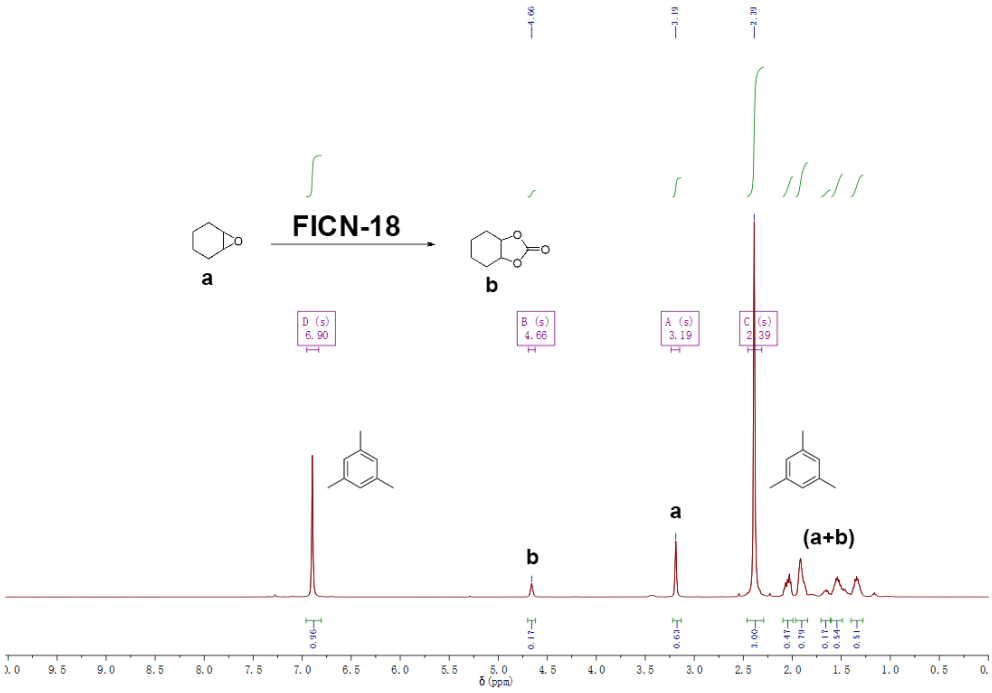

Figure S25. ^{1}H-NMR ($CDCl_3$) spectrum for crude reaction mixture of CO_2/cyclohexene oxide cycloaddition catalyzed by FICN-18.

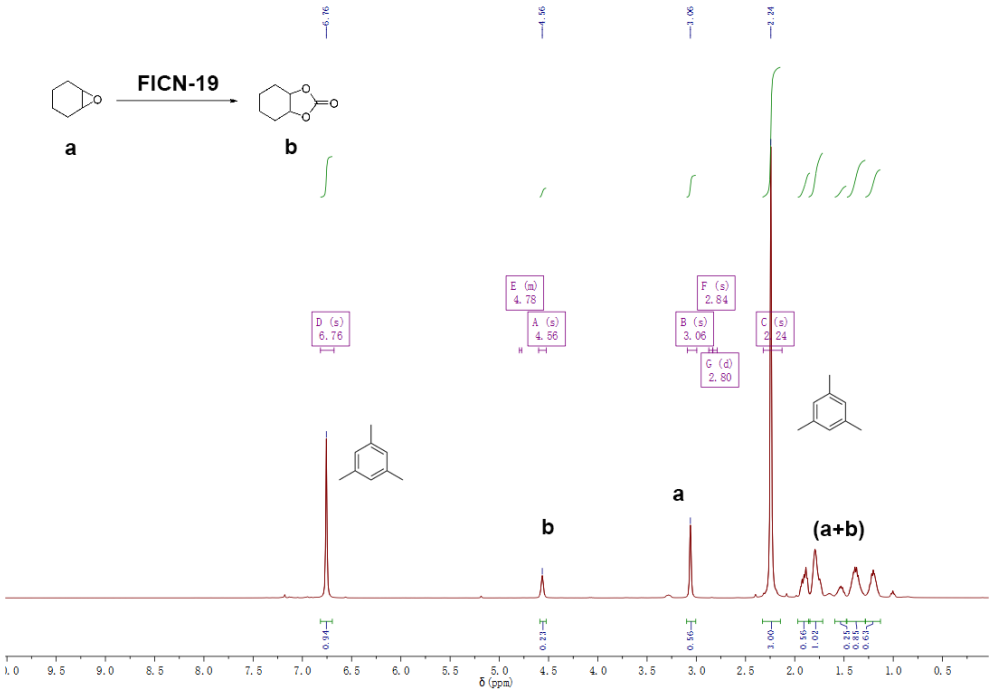

Figure S26. ^{1}H-NMR ($CDCl_3$) spectrum for crude reaction mixture of CO_2/cyclohexene oxide cycloaddition catalyzed by FICN-19.

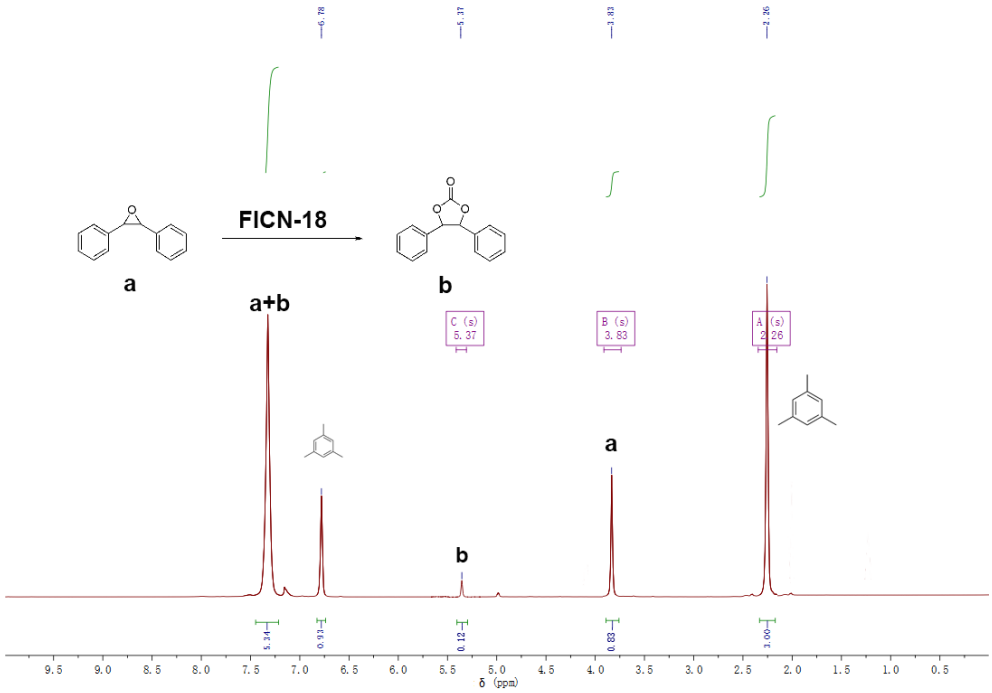

Figure S27. ^{1}H-NMR ($CDCl_3$) spectrum for crude reaction mixture of CO_2/stilbene oxide cycloaddition catalyzed by FICN-18.

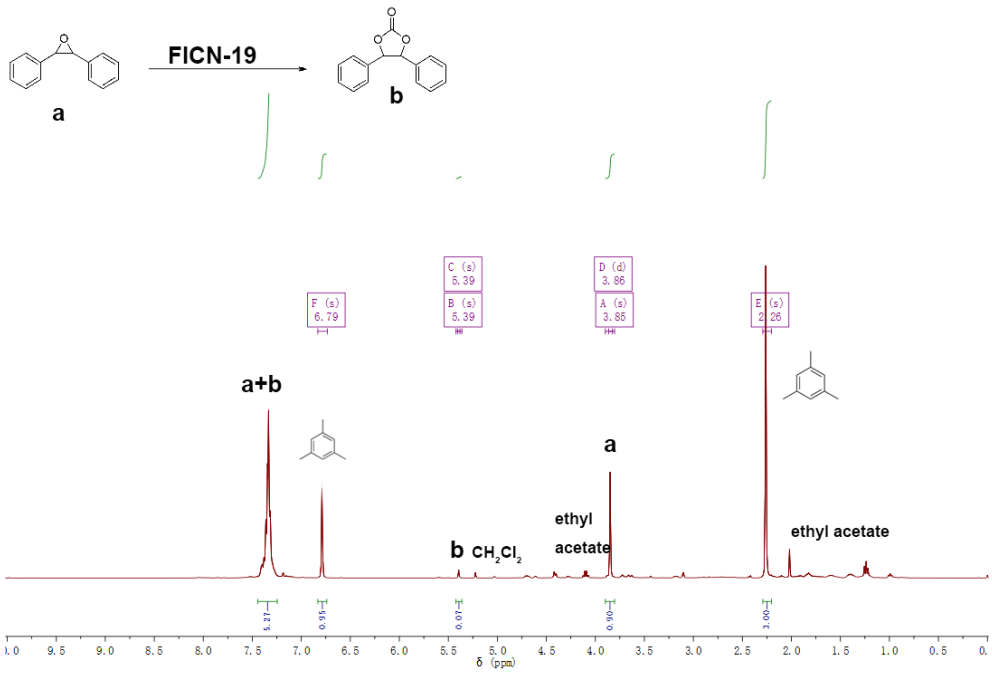

Figure S28. ^{1}H-NMR ($CDCl_3$) spectrum for crude reaction mixture of CO_2/stilbene oxide cycloaddition catalyzed by FICN-19.

9. References

1. F.-X. Ma, F.-Q. Mi, M.-J. Sun, T. Huang, Z.-A. Wang, T. Zhang and R. Cao, *Inorg. Chem. Front.*, 2022, **9**, 1812-1818.
2. S. Yuan, J. S. Qin, J. Li, L. Huang, L. Feng, Y. Fang, C. Lollar, J. Pang, L. Zhang, D. Sun, A. Alsalme, T. Cagin and H. C. Zhou, *Nat. Commun.*, 2018, **9**, 808.

3. D. Feng, W.-C. Chung, Z. Wei, Z.-Y. Gu, H.-L. Jiang, Y.-P. Chen, D. J. Darensbourg and H.-C. Zhou, *J. Am. Chem. Soc.*, 2013, **135**, 17105-17110.
4. X. L. Lv, K. Wang, B. Wang, J. Su, X. Zou, Y. Xie, J. R. Li and H. C. Zhou, *J. Am. Chem. Soc.*, 2017, **139**, 211-217.
5. K. Wang, X. L. Lv, D. Feng, J. Li, S. Chen, J. Sun, L. Song, Y. Xie, J. R. Li and H. C. Zhou, *J. Am. Chem. Soc.*, 2016, **138**, 914-919.
6. T. He, Z. Huang, S. Yuan, X. L. Lv, X. J. Kong, X. Zou, H. C. Zhou and J. R. Li, *J. Am. Chem. Soc.*, 2020, **142**, 13491-13499.
7. Y. Qin, C. Cheng, H. Geng, C. Wang, W. Hu, W. Xu, Z. Shuai and D. Zhu, *Phys Chem Chem Phys*, 2016, **18**, 14094-14103.
8. V. Colombo, S. Galli, H. J. Choi, G. D. Han, A. Maspero, G. Palmisano, N. Masciocchi and J. R. Long, *Chem. Sci.*, 2011, **2**, 1311-1319.
9. Z. Wang, A. Bilegsaikhan, R. T. Jerozal, T. A. Pitt and P. J. Milner, *ACS Appl Mater Interfaces*, 2021, **13**, 17517-17531.
10. D. W. Feng, T. Lei, M. R. Lukatskaya, J. Park, Z. H. Huang, M. Lee, L. Shaw, S. C. Chen, A. A. Yakovenko, A. Kulkarni, J. P. Xiao, K. Fredrickson, J. B. Tok, X. D. Zou, Y. Cui and Z. A. Bao, *Nature Energy*, 2018, **3**, 30-36.
11. J. Hu, X. Deng, H. Zhang, Y. Diao, S. Cheng, S. L. Zheng, W. M. Liao, J. He and Z. Xu, *Inorg. Chem.*, 2021, **60**, 161-166.
12. S. Galli, A. Maspero, C. Giacobbe, G. Palmisano, L. Nardo, A. Comotti, I. Bassanetti, P. Sozzani and N. Masciocchi, *J. Mater. Chem. A*, 2014, **2**, 12208-12221.
13. G. R. Si, X. J. Kong, T. He, W. Wu, L. H. Xie and J. R. Li, *Chinese Chemical Letters*, 2021, **32**, 918-922.
14. G. R. Si, W. Wu, T. He, Z. C. Xu, K. C. Wang and J. R. Li, *Acs Materials Letters*, 2022, **4**, 1032-1036.
15. W. Y. Gao, L. Wojtas and S. Ma, *Chem. Commun.*, 2014, **50**, 5316-5318.
16. M. Wang, J. Liu, J. Jin, D. Wu, G. P. Yang, W. Y. Zhang and Y. Y. Wang, *Crystengcomm*, 2021, **23**, 663-670.
17. Y. Z. Li, G. D. Wang, H. Y. Yang, L. Hou, Y. Y. Wang and Z. H. Zhu, *Inorg. Chem. Front.*, 2020, **7**, 746-755.
18. X. Sun, J. Gu, Y. Yuan, C. Yu, J. Li, H. Shan, G. Li and Y. Liu, *Inorg. Chem.*, 2019, **58**, 7480-7487.
19. G. Wang, C. Xu, L. Wang and W. Liu, *Dalton Trans.*, 2018, **47**, 12711-12717.
20. H. Xu, B. Zhai, C. S. Cao and B. Zhao, *Inorg. Chem.*, 2016, **55**, 9671-9676.
21. H. Beyzavi, R. C. Klet, S. Tussupbayev, J. Borycz, N. A. Vermeulen, C. J. Cramer, J. F. Stoddart, J. T. Hupp and O. K. Farha, *J. Am. Chem. Soc.*, 2014, **136**, 15861-15864.
22. Y. T. Zheng, X. Q. Wang, C. Liu, B. Q. Yu, W. L. Li, H. L. Wang, T. T. Sun and J. Z. Jiang, *Inorg. Chem. Front.*, 2021, **8**, 2880-2888.
23. L. Wang, C. Xu, Q. Han, X. Tang, P. Zhou, R. Zhang, G. Gao, B. Xu, W. Qin and W. Liu, *Chem. Commun.*, 2018, **54**, 2212-2215.
24. J. Liu, G. Yang, Y. Liu, D. Zhang, X. Hu and Z. Zhang, *Green Chem.*, 2020, **22**, 4509-4515.
25. P. T. K. Nguyen, H. T. D. Nguyen, H. N. Nguyen, C. A. Trickett, Q. T. Ton, E. Gutierrez-Puebla, M. A. Monge, K. E. Cordova and F. Gandara, *ACS Appl Mater Interfaces*, 2018, **10**, 733-744.
26. B. B. Lu, J. Yang, Y. Y. Liu and J. F. Ma, *Inorg. Chem.*, 2017, **56**, 11710-11720.

27. F. Y. Tang, J. A. Hou, K. X. Liang, J. H. Huang and Y. N. Liu, *Eur. J. Inorg. Chem.*, 2018, **2018**, 4175-4180.
28. S. Subramanian, J. Oppenheim, D. Kim, T. S. Nguyen, W. M. H. Silo, B. Kim, W. A. Goddard and C. T. Yavuz, *Chem*, 2019, **5**, 3232-3242.